Recyclable high-performance glass-fiber/epoxy composites with UV-shielding and intrinsic damage self-reporting properties

Haojie Gong, Jianqiao Wu, Zihan Zhao, Zhongkai Guo, Liang Gao, Baoyan Zhang, Min-Hui Li, Jun Hu

Chemical Engineering Journal

Recyclable High-Performance Glass-Fiber/Epoxy Composites with UV-Shielding and Intrinsic Damage Self-Reporting Properties

--Manuscript Draft--

Manuscript Number:	CEJ-D-22-06481R2
Article Type:	Research Paper
Keywords:	glass-fiber-reinforced composites; damage self-reporting material; disulfide bonds; mechanochromic; UV-shielding; recycling
Corresponding Author:	Jun Hu, Ph.D Beijing University of Chemical Technology Beijing, Beijing CHINA
First Author:	Haojie Gong
Order of Authors:	Haojie Gong
	Jianqiao Wu
	Zihan Zhao
	Zhongkai Guo
	Liang Gao
	Baoyan Zhang
	Min-Hui Li
	Jun Hu, Ph.D
Abstract:	Predicting the barely visible damage on high-performance glass-fiber-reinforced composites (GFRCs) is of vital importance, as it can mitigate catastrophic material failure and hence, help save costs and lives if GFRCs are used as structural parts. However, the use of current damage self-reporting GFRCs often involves complicated modifications of the matrix or fibers, further, interfacial defect generation and poor resulting mechanical properties may be inevitable when extrinsic mechanochromic additives are employed. In this study, a disulfide bond-tailored epoxy matrix for GFRCs was synthesized from the diglycidyl ester of aliphatic cyclo (DGEAC) and 4,4-dithiodianiline (AFD), which possessed sufficient solvent resistance, good thermal/mechanical performance (Tg ≥ 206 °C, tensile strength ≈ 70 MPa), and UV-shielding properties. Owing to the exchange reaction of disulfide bonds and dynamic transesterification reactions catalyzed by internal tertiary amines, the DGEAC/AFD networks could topologically rearrange, and were easily degraded by dithiothreitol (DTT). More importantly, the DGEAC/AFD networks showed intrinsic mechanochromic properties upon damage due to the formation of sulfenyl radicals. This indicated that the GF/DGEAC/AFD composites were damaged, which was manifested by the appearance of colors visible to the naked eye (a kind of self-reporting mechanism). In this case, the degree of damage could be accurately determined, providing a pre-indication of material failure. In addition, benefiting from the good comprehensive performance of the DGEAC/AFD matrix, the GF/DGEAC/AFD composites exhibited outstanding mechanical properties (tensile strength of approximately 470 MPa and flexural strength of approximately 726 MPa). Meanwhile, the glass fibers (GFs) could be completely recycled in a non-destructive manner by immersing the GF/DGEAC/AFD composites in a solution of DTT. The work presents an interesting example on the synthesis of high-performance, pre-damage-indicative, and recyclable GFRCs.
Response to Reviewers:	Dear Prof. Todd Hoare, With this letter we submit our revised manuscript (Manuscript ID: CEJ-D-22-06481R1) as required to Chemical Engineering Journal. We would like to thank the editors and the reviewers for all suggestions and insightful comments, which have been extremely beneficial for us to revise the manuscript and make it more acceptable to the general audience. We have taken all suggestions into account, and hope that the responses will clarify the questions. Detailed responses are attached, and all the changes in our

	revised manuscript are highlighted in yellow color. We confirm that the figures and tables in Manuscript and Supplementary data are the original works. Your kind consideration of our revised manuscript is highly appreciated. Sincerely yours, Jun Hu, Ph.D, Professor Beijing Advanced Innovation Center for Soft Matter Science and Engineering Beijing University of Chemical Technology Beijing 100029, China Email: jhu@mail.buct.edu.cn

Recyclable High-Performance Glass-Fiber/Epoxy Composites with UV-Shielding and Intrinsic Damage Self-Reporting Properties

Haojie Gong[a], Jianqiao Wu[a,b], Zihan Zhao[a], Zhongkai Guo[a], Liang Gao[c], Baoyan Zhang[c], Min-Hui Li*[a,d], and Jun Hu*[,a]

[a]Beijing Advanced Innovation Center for Soft Matter Science and Engineering, Beijing University of Chemical Technology, Beijing 100029, China

[b]College of Materials and Chemical Engineering, Chuzhou University, West Huifeng Road 1, Langya District, Chuzhou 239000, China

[c]Department of Resin & Prepreg, AVIC Manufacturing Technology Institute Composite Technology Center, Shijun Road 1, Shunyi District, Beijing 101300, China

[d]Chimie ParisTech, PSL University, CNRS, Institut de Recherche de chimie, Paris 75005, France

*Corresponding authors

Email: jhu@mail.buct.edu.cn (Jun Hu), min-hui.li@chimieparistech.pls.eu (Min-Hui Li)

Abstract

Predicting the barely visible damage on high-performance glass-fiber-reinforced composites (GFRCs) is of vital importance, as it can mitigate catastrophic material failure, and hence, help save costs and lives if GFRCs are used as structural parts. However, the use of current damage self-reporting GFRCs often involves complicated modifications of the matrix or fibers, further, interfacial defect generation and poor resulting mechanical properties may be inevitable when extrinsic mechanochromic additives are employed. In this study, a disulfide bond-tailored epoxy matrix for GFRCs was synthesized from the diglycidyl ester of aliphatic cyclo (DGEAC) and 4,4-dithiodianiline (AFD), which possessed sufficient solvent resistance, good thermal/mechanical performance ($T_g \geq 206$ °C, tensile strength ≈ 70 MPa), and UV-shielding properties. Owing to the exchange reaction of disulfide bonds and dynamic transesterification reactions catalyzed by internal tertiary amines, the DGEAC/AFD networks could topologically rearrange, and were easily degraded by dithiothreitol (DTT). More importantly, the DGEAC/AFD networks showed intrinsic mechanochromic properties upon damage due to the formation of sulfenyl radicals. This indicated that the GF/DGEAC/AFD composites were damaged, which was manifested by the appearance of colors visible to the naked eye (a kind of self-reporting mechanism). In this case, the degree of damage could be accurately determined, providing a pre-indication of material failure. In addition, benefiting from the good comprehensive performance of the DGEAC/AFD matrix, the GF/DGEAC/AFD composites exhibited outstanding mechanical properties (tensile strength of approximately 470 MPa and flexural strength of approximately 726 MPa). Meanwhile, the glass fibers (GFs) could be completely recycled in a non-destructive manner by immersing the GF/DGEAC/AFD composites in a solution of DTT. The work presents an interesting example on the synthesis of high-performance, pre-damage-indicative, and recyclable GFRCs.

Keywords: glass-fiber-reinforced composites; damage self-reporting material; disulfide bonds; mechanochromic; UV-shielding; recycling

1. Introduction

Owing to their low weight, high strength, high stiffness, and corrosion resistance, glass-fiber-reinforced composites (GFRCs) are widely used in the aerospace industry, and for wind power generation, construction engineering, and high-tech manufacturing [1]. During the service life of GFRCs, predicting and sensing barely visible damage in complex environments is of vital importance, as it can mitigate catastrophic material failure, and hence, save costs and lives if the GFRCs are used as structural parts [2]. At present, the frequently used non-destructive testing methods in the industry include visual inspection [3], piezoelectric sensing [4], acoustic emission [5-7], optical coherence tomography [8, 9], shearography [10-12], pulsed phase thermography [13], and X-ray/γ-ray analysis [14]. Despite the effectiveness of these methods, it is assumed that the damage location has been identified visually first. This assumption makes these methods suitable only for post-damage analysis, which is costly and time-consuming. Therefore, the development of GFRCs that can autonomously self-report damage over time has attracted increasing attention in recent years. To date, self-reporting GFRCs containing dye-filled vascular networks [15-17], microcapsules and hollow fibres [18-23], and mechanochromic additives [24-26] have been developed. For example, Sottos and co-workers encapsulated 2′,7′-dichlorofluorescein into double-shell-walled polyurethane/poly(ureaformaldehyde) microcapsules, which could clearly identify a crack as small as 10 μm in width on the surface of the composite under normal light [20]. Kling et al. infiltrated thin hollow glass fibers (GFs) with polyester curing agents and rhodamine B as an indicator, and they added a white dye to color the matrix and mask the fluorescent color of rhodamine B in the undamaged state. Upon damage,

rhodamine B migrated to the surface of the composites and the damage location was visualised using a UV lamp [23]. In contrast, Adelung et al. used a mechanochromic spiropyran additive in a polythiourethane matrix. Spiropyran moieties can rapidly self-report the damage degree of GFRCs through their force-induced covalent bond fracture [26]. However, these studies often involved complicated modifications of fibers or matrices. Moreover, interfacial defects might inevitably occur and poor mechanical properties might result if extrinsic mechanochromic additives are employed. Hence, the fabrication of high-performance GFRCs that can intrinsically self-report damage by naked-eye visualisation without complicated modifications to the fibers and matrix is still a major challenge.

Carbon neutrality and circular economy are topical concepts owing to the growing concerns associated with the oil crises and environmental issues. Extensive efforts have been invested to recycle materials. However, the permanently cross-linked networks of the thermoset matrix in conventional GFRCs make their recycling difficult once they are damaged or unusable. To date, the most commonly used recycling technologies for GFRCs are mechanical recycling [27-29] and pyrolysis recycling [30-32]. Mechanical recycling often produces small pieces of low value, which are then used as fillers in composites or combustible materials. On the other hand, the high-temperature and high-pressure conditions of pyrolysis recycling are too harsh and may potentially pose safety hazards in industrial production. It is important to address all these issues in current GFRC recycling technologies for sustainable development in modern society. The use of covalent adaptable networks (CANs) in the GFRC matrix is a promising solution.

CANs, pioneered by Bowman and co-workers in 2010 [33], are three-dimensional cross-linked networks that contain a sufficient number and topology of reversible covalent bonds to enable the cross-linked network structure to respond chemically to an applied stimulus, such as

heat [34], light [35], or pH [36], and to achieve network rearrangement. These dynamic covalent bonds include ester bonds [34, 37], acetal linkages [38], imine bonds [39], and disulfide bonds [40, 41], which have been introduced into diverse resin materials to enable their recyclability. Among these, the disulfide bond is considered to be one of the most promising dynamic bonds. Typically, a catalyst is not required during bond exchange, thereby mitigating the phase separation and performance deterioration of the composites. On the other hand, the cleavage of disulfide bonds can generate sulfenyl radicals that are visible to the naked eye. Therefore, when composites are subjected to external damage, the damage can be revealed at the molecular level by the color change due to the cleavage of disulfide bonds in the matrix without the use of any dye-modified additives [42]. Taking advantage of this phenomenon, in this study, we prepared recyclable high-performance GFRCs using the commercially available diglycidyl ester of aliphatic cyclo (DGEAC) and 4,4-dithiodianiline (AFD) as the matrix and GFs of EW250F as reinforcing fibers (**Scheme 1**). The cured DGEAC/AFD networks offered sufficient solvent resistance, good thermal properties ($T_g \geq 206$ °C), and mechanical properties (tensile strength of ~ 70 MPa) comparable to those of conventional epoxy thermosets. Moreover, they exhibited UV-shielding, stress relaxation at high temperatures (200 °C), degradation by the reduction agent dithiothreitol (DTT), and intrinsic mechanochromic features due to the cleavage of disulfide bonds. The laminate samples of the GF/DGEAC/AFD composites showed superior mechanical robustness (tensile strength ≈ 470 MPa and flexural strength ≈ 726 MPa) and damage self-reporting ability due to the intrinsic mechanochromic features of the matrix. Therefore, the degree of damage caused by impact could be evaluated accurately, providing an indication of material failure. Finally, the GFs could be completely recycled by immersing the GF/DGEAC/AFD composites in a solution of DTT, because

the thiol groups and hydroxyl groups of DTT participated in the exchange reactions and the networks were destroyed. Thus, the GFs showed properties identical to those of the original GFs.

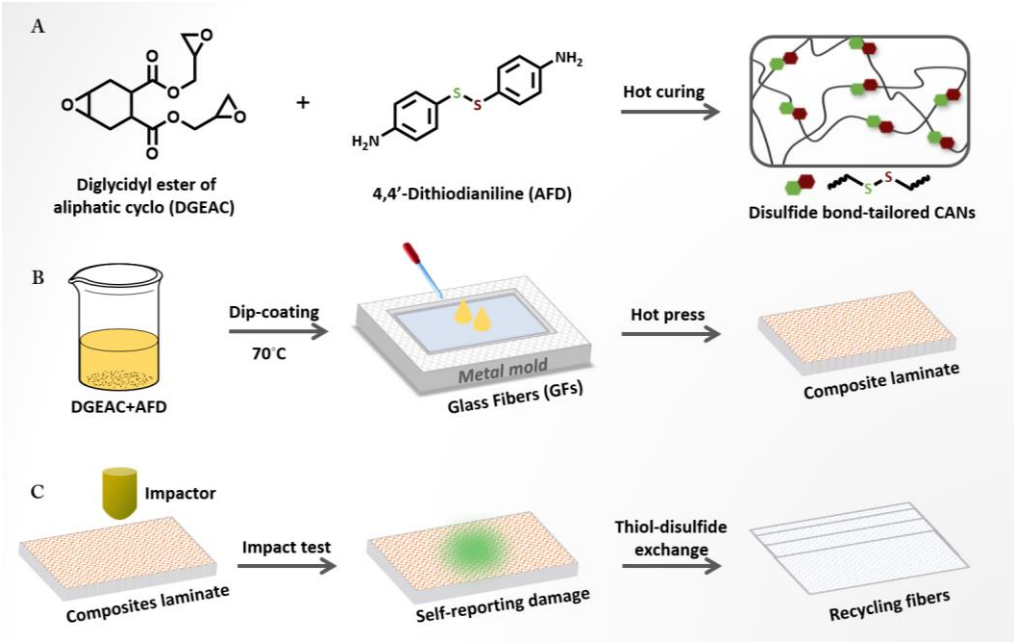

Scheme 1. Schematics of (A) synthesis of the cross-linked DGEAC/AFD networks, (B) preparation of GF/DGEAC/AFD composites, and (C) intrinsic damage self-reporting by GF/DGEAC/AFD composites and recycling of GFs.

2. Experimental section

2.1 Materials

Diglycidyl ester of aliphatic cyclo (DGEAC, Tianjin Jindong Chemical Factory), 4,4-dithiodianiline (AFD, Energy Chemical), aniline (Amethyst Chemical), dithiothreitol (DTT, Energy Chemical), and woven glass fiber (GFs) (EW250F, Nanjing Glass Fiber-Research and Design Institute) were used as purchased, without further purification.

2.2 Synthesis of the cross-linked DGEAC/AFD and DGEAC/aniline networks

Certain amounts of AFD and DGEAC were initially mixed at 50 °C and degassed under vacuum. Subsequently, the homogeneous viscous liquid was poured into a mold. Followed by

curing in an oven at 100 °C for 1 h, 150 °C for 4 h, and 180 °C for 2 h, the cross-linked DGEAC/AFD networks were prepared with stoichiometric ratios of 0.5, 0.6, and 0.7 (R = amine/epoxy groups). The reference epoxy network of DGEAC/aniline was synthesized similarly. Initially, certain amounts of aniline and DGEAC were mixed at 70 °C and degassed under vacuum. Subsequently, the homogeneous viscous liquid was poured into a mold followed by curing at 110 °C for 1 h, 150 °C for 4 h, and 180 °C for 2 h in an oven, thus affording the cross-linked DGEAC/aniline networks (amine/epoxy groups = 0.5).

2.3 Preparation of GF/DGEAC/AFD composites

Initially, AFD (3.75 g, 15.08 mmol) and DGEAC (6.00 g, 20.11 mmol) were mixed at 50 °C and degassed under vacuum to obtain a homogeneous solution. Subsequently, four slices of woven GFs were dip-coated by the solution layer-by-layer at 70 °C, with a GF weight fraction of approximately 71%. The coated woven fabric was then placed in a stainless mold (80 mm × 60 mm × 1 mm) and cured at 100 °C for 1 h, 150 °C for 4 h, and 180 °C for 2 h at a pressure of 10 tons.

2.4 Characterization

Rheological measurement. The rheological behavior of DGEAC/AFD blends was studied in oscillatory mode using a Discovery HR-1 rheometer (TA Instruments) equipped with parallel aluminum plates (diameter 25 mm). Oscillation temperature ramp measurements were performed from 25 to 180 °C with a strain of 1%, an angular frequency of 1 Hz, and a heating rate of 5 °C/min. One temperature point was selected according to the viscosity curve in the heating state, and then the viscosity-time curve in the constant temperature state was measured.

Differential scanning calorimetry (DSC) test. A differential scanning calorimeter (TA-DSC25) was used to investigate the curing behavior. Samples (~ 5 mg) were sealed in aluminum

crucibles and scanned at a heating rate of 5 °C/min to cure them. The cured samples (~ 5 mg) were heated from 25 to 250 °C at a heating rate of 10 °C/min.

Fourier-transform infrared (FTIR) spectroscopy. The samples were scanned from 4000 to 600 cm^{-1} using a spectrophotometer (Bruker V70) equipped with an ATR probe.

Swelling test. The swelling ratios were measured by immersing the samples (~ 30 mg, m_0) sequentially in acetonitrile, tetrahydrofuran, acetone, and ethyl acetate at room temperature. Upon reaching equilibrium, the samples were removed from the solution. The excess solvent on the surface was removed with filter paper, and the swollen samples were weighed (m_1). The swelling ratio was calculated using the following equation:

$$Swelling\ ratio\ (\%) = \frac{m_1 - m_0}{m_0} \times 100\% \quad (1)$$

Gel content test. The samples (~ 30 mg, m_0) were sequentially immersed in acetonitrile, tetrahydrofuran, acetone, and ethyl acetate at room temperature for 20 h, respectively. Each sample was then dried in a vacuum oven at 70 °C and weighed (m_1). The gel content was calculated using the following equation:

$$Gel\ content\ (\%) = \frac{m_1}{m_0} \times 100\% \quad (2)$$

Solvent resistance. The samples (10 mm × 10 mm × 1.5 mm) were sequentially immersed in ethanol, methanol, tetrahydrofuran, acetone, toluene, chloroform, NaOH (1 M), HCl (1 M), H_2SO_4 (1 M), H_2O, and N, N-dimethylformamide (DMF) for 2 weeks to investigate the solvent resistance.

Dynamic mechanical analysis (DMA). The dynamic mechanical properties were measured using a dynamic mechanical analyzer (TA-Q850) in the tension mode. Samples with dimensions of 30 mm × 5 mm × 1.5 mm were scanned from 25 to 250 °C at a heating rate of 3 °C/min. The amplitude was set at 10 μm and the frequency was 1 Hz.

Thermogravimetric analysis (TGA). The thermal stability was measured using a thermogravimetric analyzer (NETZSCH-STA449F3). The samples (~ 5 mg) were loaded into alumina crucibles and scanned from 25 to 800 °C at a heating rate of 10 °C/min under a N_2 atmosphere.

Tensile test. The tensile properties of the cross-linked DGEAC/AFD networks were measured using an electromechanical universal testing machine (ETM504C, Hubei Wance Test Machine Co. Ltd., China) at room temperature according to the UNE-EN-ISO 527 standard using dumbbell-shaped specimens at a stretching speed of 2 mm/min. For the GF/DGEAC/AFD composites, rectangular specimens with dimensions of 60 mm × 15 mm × 1 mm were used for the test at a stretching speed of 5 mm/min. At least five samples were tested.

UV-Vis spectroscopy. The UV-shielding performance of the DGEAC/AFD film was measured using a UV-vis spectrophotometer (G-9, Nanjing PKILES) from 200 to 1000 nm. The UV-vis spectra of the DGEAC/AFD powder generated by scraping the film with a knife were recorded using a spectrophotometer (UV-2600, Shimadzu).

Stress relaxation test. The stress relaxation was measured using a dynamic mechanical analyzer (TA-Q850). A sample with dimensions of 30 mm × 5 mm × 1.5 mm was heated to the prescribed temperature and soaked for 10 min. Subsequently, an instantaneous strain of 1% was applied. The stress and modulus were measured for several hours until equilibrium was achieved.

Creep recovery test. The creep recovery behavior was measured using a dynamic mechanical analyzer (DMTA-V). A sample with dimensions of 30 mm × 5 mm × 1.5 mm was heated to 200 °C and soaked for 10 min. After applying a constant force (0.5 MPa) for 1 h, the stress was removed, and the sample was allowed to recover for another 1 h.

Electron paramagnetic resonance (EPR) spectroscopy. The EPR experiments were performed using an EPR spectrometer (Bruker E500) at 25 °C using a microwave frequency of 9.64 GHz, microwave power of 10 mW, and modulation amplitude of 100 kHz. The *g*-value was calculated according to the equation: $h\nu = g\beta B$, where h is Planck's constant, ν is the frequency, β is the Bohr magneton, and B is the magnetic field.

Raman spectroscopy. Raman spectra were recorded using a LabRAM HR Evolution spectrograph using laser irradiation of 785 nm wavelength, an exposure time of 90 s, and a laser energy of 10 mW.

X-ray 3D microscopy. An X-ray 3D microscope (Nano Voxe 12000) was used to observe the internal structure of the GF/DGEAC/AFD composites. Samples with dimensions of 10 mm × 10 mm × 1 mm were used for the tests.

'Hammer impact' test. This test involved the use of a hammer that could freely fall on a composite specimen fixed on a rectangular platform. Specifically, a specimen with dimensions of 20 mm × 20 mm × 1 mm was impacted by a hammer weighing 0.498 kg that was dropped from a height of 120 mm (~ 0.598 J of energy per impact). This test was repeated periodically until the composite failed. The impact energy required to change the color and damage the composites was determined by the number of impacts. An image was captured after each impact to track the color change and failure of the GF/DGEAC/AFD composites. Moreover, a blue color channel contribution in these images was generated using ImageJ software for quantitative analysis. The corresponding video was produced by stacking the images together.

Degradation test. The DGEAC/AFD matrix (~ 20 mg, m_0) and GF/DGEAC/AFD composites (~ 40 mg, m_0) were immersed in a DTT/DMF solution (0.02 g/mL) at 70 °C, respectively. The samples were removed from the solution after different degradation times, then dried at 150 °C for

24 h, and weighed (m_1). At least three replicate tests were performed at each time point. The relative weights were calculated using the following equation:

$$Relative\ weight\ (\%) = \frac{m_1}{m_0} \times 100\% \quad (3)$$

The cleavage planes of the GF/DGEAC/AFD composites during degradation were observed using scanning electron microscopy (SEM, JSM-7610F, Japan) with an accelerating potential of 5 kV. The morphologies and chemical compositions of the recycled and virgin GFs were investigated by SEM and SEM-EDS (EDS: energy-dispersive X-ray spectroscopy).

3. Results and discussion

3.1 Synthesis and characterization of the DGEAC/AFD networks

As viscosity is an important parameter to evaluate the curing and processability of epoxy resin, the rheological experiments of DGEAC/AFD blends at different stoichiometric ratios (R = 0.5, 0.6, and 0.7, amine/epoxy group) were performed. **Fig. S1A** shows the viscosity-temperature curves with a heating rate of 5 °C/min. Initially, when the temperature is low (25 ~ 60 °C), the curing degree is low and the physical change of viscosity is dominant, so the viscosity drops rapidly with the rise of temperature at this stage. Subsequently, as the temperature increases continuously, the curing reaction gradually takes place, making the viscosity achieve an equilibrium at a low level (~ 0.04 Pa.s) within a temperature range from 60 to 150 °C. Finally, the curing reaction intensifies in the high temperature range (> 150 °C), where the chemical change becomes the dominant factor promoting the sharp increase of viscosity. According to these viscosity-temperature curves, 110 ºC was chosen to investigate their isothermal viscosity behaviors. As shown in **Fig. S1B**, the viscosity-time curves are similar for R = 0.5, 0.6, and 0.7, where the viscosity increases slowly at the beginning of the test, presenting a low viscosity plateau, while an exponential rise in viscosity occurs with the extension of time as the curing degree increases sharply. The time corresponding to the low viscosity platform ($\leqslant$ 0.8 Pa.s) is 1618 s,

1353 s, and 1216 s for R = 0.5, 0.6, and 0.7, respectively. The curing processes of DGEAC/AFD blends were further investigated using DSC at a heating rate of 5 °C/min from 50 to 220 °C. In **Fig. 1A**, clear exothermic peaks are observed at approximately 150 °C, and the reaction enthalpies (ΔH) are 419 J/g, 371 J/g, and 331 J/g for R values of 0.5, 0.6, and 0.7, respectively. The declining trend of ΔH from R = 0.5 to 0.7 indicates that the curing degree at R = 0.5 is the highest [43]. To cover the temperature range of the curing reaction and avoid the degradation of the raw materials, the following curing profiles were designed: 100 °C for 1 h, 150 °C for 4 h, and 180 °C for 2 h. The cured DGEAC/AFD was transparent and mechanically strong as shown in **Fig. 1B**. To confirm the formation of cross-linked networks, the FTIR spectra of monomers and cured DGEAC/AFD were acquired **(Fig. 1C**, **1D)**. The peaks at 3056 and 905/853 cm^{-1} were assigned to epoxy groups, whereas the signals at 1740 and 2925/2853 cm^{-1} belonged to ester bonds and methylene groups, respectively, from DGEAC. For AFD, the peaks at 3417/3331 cm^{-1} and 1624 cm^{-1} corresponded to amine stretching and bending vibrations, and the signals at 1587 and 1494 cm^{-1} corresponded to benzene ring vibrations. After curing, the epoxy peaks disappeared, and a new hydroxyl peak at 3434 cm^{-1} emerged, with the remaining ester bonds at 1740 cm^{-1}, indicating the curing reaction was complete. Evidence from DSC further confirmed the complete curing, as no residual curing peak was observed (**Fig. 1E**). In contrast, the glass transition of the networks was clearly observed without peaks related to melting, demonstrating the amorphous nature of the DGEAC/AFD networks, which is in accordance with their high transparency. The gel content and swelling ratio are two important references for characterizing the integrity of cross-linked networks, as they can directly reflect the extent of cross-linking [44]. All DGEAC/AFD networks exhibited a high gel content (> 99%) and low swelling ratio (**Fig. 1F**, **Table S1**), implying that the networks were completely cross-linked. In addition, the DGEAC/AFD (R = 0.5) was selected to evaluate the

solvent resistance. After sequentially immersing in ethanol (EtOH), methanol (MeOH), tetrahydrofuran (THF), acetone (Act.), toluene (PhMe), chloroform ($CHCl_3$), NaOH (1 M), HCl (1 M), H_2SO_4 (1 M), H_2O, and N, N-dimethylformamide (DMF) for 2 weeks at room temperature, all DGEAC/AFD pieces remained intact (**Fig. 1G**), indicating that DGEAC/AFD had good resistance to organic solvents and acidic and alkaline aqueous solutions. In summary, a cross-linked network of DGEAC/AFD was completely formed with sufficient solvent resistance.

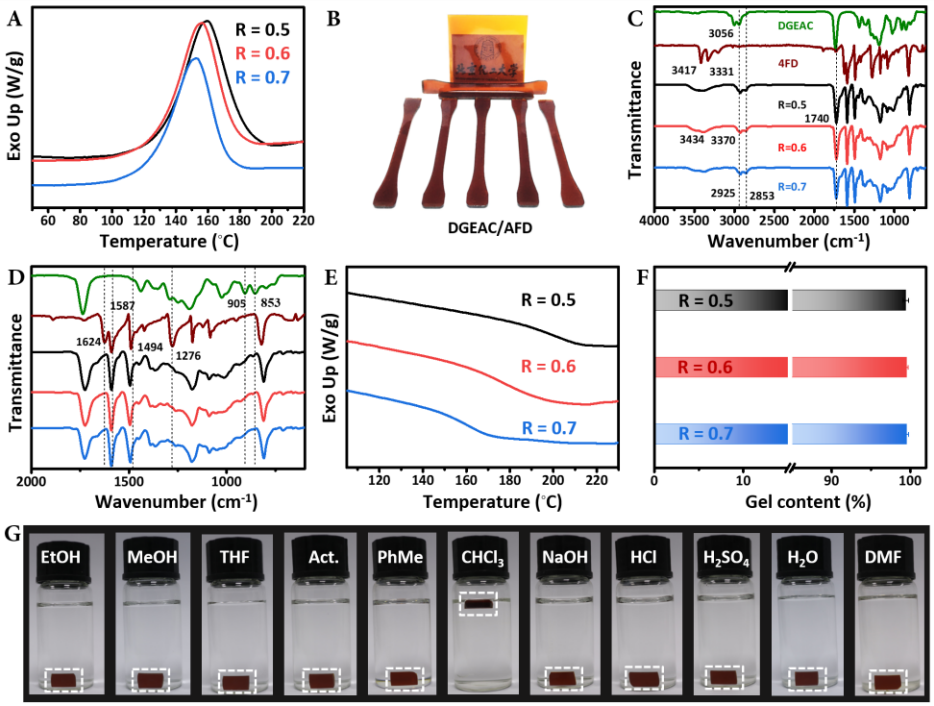

Fig. 1. (A) DSC curves of the DGEAC/AFD mixtures at a heating rate of 5 °C/min. (B) Digital photos of DGEAC/AFD networks. (C, D) FTIR spectra of DGEAC, AFD, and DGEAC/AFD networks. (E) DSC curves of DGEAC/AFD networks at a heating rate of 10 °C/min. (F) Gel content of DGEAC/AFD networks. (G) Digital photos of DGEAC/AFD networks after immersion in different solvents for 2 weeks at room temperature.

3.2 Thermal, mechanical, and UV-shielding properties of DGEAC/AFD networks

The dynamic mechanical properties of the DGEAC/AFD networks are presented in **Fig. 2A** and **Table 1**. All transitions from the glassy state to the rubbery state occur at temperatures higher than 180 °C, with storage modulus at 30 °C of 4859, 3616, and 3436 MPa for R values of 0.5, 0.6, and 0.7, respectively, demonstrating the good rigidity of the DGEAC/AFD networks. The tan δ peaks at 212, 209, and 206 °C are assigned to the corresponding T_g values, and indicate that T_g slightly decreases from R values of 0.5 to 0.7. In general, the T_g of cross-linked polymers is determined by the cross-linking density and rigidity of the chain segments [45]. According to Flory's rubber elasticity theory, the cross-linking density (v_e) of the DGEAC/AFD networks was calculated using equation (4) [46, 47]:

$$E' = 3v_eRT \qquad (4)$$

where E' is the storage modulus in the rubbery state at T_g + 30 °C, R is the gas constant, and T is the Kelvin temperature of T_g + 30 °C. As shown in **Table 1**, although the stiffness of the DGEAC/AFD network increases from R values of 0.5 to 0.7, the corresponding v_e decreases from 3097 to 2395 and 1732 mol/m^3, respectively. Consequently, this equilibrium leads to a slight decrease in T_g. The T_g values measured using DSC in **Fig. 1E** show a similar trend. In addition, DGEAC/AFD networks exhibit good damping performance, with a higher tan δ (> 0.7) and better damping property.

The thermal stabilities of the networks were characterised using TGA, where the temperatures at 5% weight loss ($T_{d5\%}$) were 282, 277, and 270 °C for R values of 0.5, 0.6, and 0.7, respectively (**Fig. 2B**, **Table 1**). The statistical heat-resistance temperature (T_s) was calculated using the following equation [48]:

$$T_s = 0.49[T_{d5\%} + 0.6(T_{d30\%}-T_{d5\%})] \qquad (5)$$

where $T_{d5\%}$ and $T_{d30\%}$ represent the temperatures at 5% and 30% weight loss, respectively. As shown in **Table S2**, T_s values of 151, 152, and 153 °C are obtained for these three networks, revealing similar thermal stabilities. Moreover, the DGEAC/AFD networks exhibit three stages of weight loss (**Fig. 2C**). Because the bond energies of the disulfide bonds are lower than those of C-C, C-O, and C-N bonds, the thermal decomposition of disulfide bonds occurs between 250 and 300 °C in the first stage [49], where the weight losses are 9.91%, 11.03%, and 12.02% for R values of 0.5, 0.6, and 0.7, respectively, similar to the theoretically calculated weights of disulfide bonds. The weight loss in the second stage (approximately 40%) mainly involves the thermal degradation of fatty chains in the networks, which occurs in the temperature range of 340–360 °C. The last weight loss stage at 410–500 °C is caused by the thermal degradation of aromatic rings [50]. All the above results suggest that the DGEAC/AFD networks possess good thermal stability for potential applications.

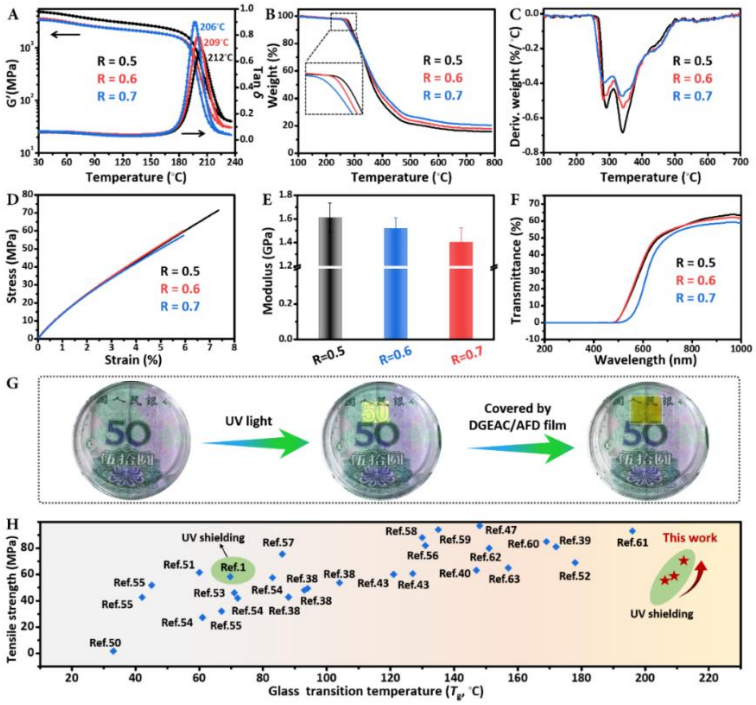

Fig. 2. (A) Storage modulus (G') and tan δ of DGEAC/AFD networks at a heating rate of 3 °C/min. (B) TGA and (C) the corresponding DTG curves of DGEAC/AFD networks at a heating rate of 10 °C/min. (D) Tensile stress-strain curves and (E) corresponding modulus of DGEAC/AFD networks. (F) Transmittance spectra of DGEAC/AFD networks in the wavelength range of 200-1000 nm. (G) Digital photos of the anti-counterfeiting logo covered by the DGEAC/AFD film (R = 0.5) under UV light at 365 nm. (H) Comparison of the comprehensive performance of DGEAC/AFD networks with those of other reported epoxy thermosets containing dynamic covalent bonds.

As an important indicator of thermoset matrices, the mechanical properties of the DGEAC/AFD networks were investigated by tensile stress-strain experiments. In **Fig. 2D**, all the networks exhibit rigid tensile behaviour without a yield point, and their mechanical properties can be adjusted by changing the AFD content in the networks. The tensile strength of the DGEAC/AFD network (R = 0.5) was the highest at 70.7 MPa, followed by values of 58.9 and 55.4 MPa for R values of 0.6 and 0.7, respectively. Correspondingly, the Young′s modulus for R = 0.5 (1.61 GPa) was also higher than that for R = 0.6 and 0.7 (**Fig. 2E**, **Table 1**), consistent with the varying trend of tensile strength.

In fields such as the aerospace industry and microelectronic packaging, insufficient UV-shielding is a hindrance for long-term use, especially in the pursuit of visible-light transparency. Therefore, it is imperative to build transparent thermoset matrices with UV-shielding capabilities. As shown in **Fig. 2F**, the transmittance of the DGEAC/AFD networks is nearly 0% from 200 to 500 nm, revealing a blocking ability over the full wavelength range of UV light. This result is intuitively verified in **Fig. 2G**. The anti-counterfeiting logo on the surface of the 50-yuan CNY fluoresces upon irradiation by a UV lamp but no longer fluoresces once covered by a

DGEAC/AFD film, which implies that DGEAC/AFD networks can be used in UV-shielding to prevent UV-caused ageing. Based on the tensile strength, T_g, and UV-shielding properties, we compared the DGEAC/AFD networks with other reported epoxy thermosets containing dynamic covalent bonds. As illustrated in **Fig. 2H** and **Table S3**, the comprehensive performance of the DGEAC/AFD networks is better than that reported in other studies.

Table 1 Composition, thermal, and mechanical properties of DGEAC/AFD networks.

Sample[a]	T_g (°C)[b]	E' (MPa)[c]	v_e (mol m^{-3})[d]	$T_{d5\%}$ (°C)[e]	Young′s modulus (GPa)[f]	Tensile strength (MPa)[f]	Elongation at break (%)[f]
R = 0.5	212	39.88	3097	282	1.61 ± 0.12	70.7±1.5	7.5 ± 1.4
R = 0.6	209	30.65	2395	277	1.51 ± 0.09	58.9±2.7	5.8 ± 0.6
R = 0.7	206	22.08	1732	270	1.40 ± 0.12	55.4±2.2	5.6 ± 1.1

[a]R represents the stoichiometric ratio of amine/epoxy groups. [b]T_g value was decided from tan δ in Fig. 2A. [c]E' was obtained from storage modulus at temperature (T_g + 30°C) in Fig. 2A. [d]v_e was calculated by equation (4). [e]$T_{d5\%}$ was obtained from TGA cures in Fig. 2B. [f]Young′s modulus, tensile strength, and elongation at break were obtained from Fig 2D.

3.3 Dynamic bond exchange and degradation of DGEAC/AFD networks

From a structural point of view, in addition to the exchange of disulfide bonds, the β-hydroxyesters and tertiary amines present in the DGEAC/AFD networks, which can accelerate the dynamic transesterification reactions (TERs). To validate this TERs, a reference epoxy resin networks, named as DGEAC/aniline, was synthesized by curing DGEAC with aniline (amine/epoxy group = 0.5, **Fig. S2A**). The DSC curve in **Fig. S2B** shows that there is a clear exothermic peak around 150 °C, which indicates that amino groups in aniline react well with the

epoxy groups. In order to ensure the complete curing of the DGEAC/aniline networks, the following curing process was designed: 110 °C for 1 h, 150 °C for 4 h, and 180 °C for 2 h. The cured DGEAC/aniline was transparent and mechanically strong as shown in **Fig. S2C**. Evidence from DSC in **Fig. S2D** confirmed the complete curing, as no residual curing peak appeared. In contrast, the glass transition plateau of the DGEAC/aniline networks was observed clearly (T_g = 136 °C). In addition, the stress relaxation characteristic of the DGEAC/aniline networks was investigated by using DMA in **Fig. S2E**, where the relaxation time (τ*), defined as the time when the modulus relaxes to 1/e of the original, decreased to 406 s from 809 s when the temperature rose from 200 to 220 °C, revealing a rapid relaxation rate of the DGEAC/aniline networks. According to these results and the reports in other works [64-66], it was proposed that tertiary amines and the adjacent hydroxyl groups would like to form a five-membered cyclic intermediate through intramolecular hydrogen bonds, which increased the nucleophilicity of hydroxyl groups and promoted the TERs, thus achieving the dynamic topological rearrangements (**Fig. S2F**).

For the DGEAC/AFD networks (R = 0.5), the stress relaxation property was evaluated at different temperatures for verifying the transesterification and disulfide exchange reactions (**Fig. S3**). The τ* was determined to be 462 s at 180 °C, 320 s at 190 °C, 156 s at 200 °C, and 28 s at 230 °C (**Fig. 3A)**. Accordingly, the activation energy (E_a) of the bond exchange reaction can be calculated using the Arrhenius equation [44]:

$$\ln \tau^* = \frac{E_a}{RT} - \ln A \qquad (6)$$

where R is the gas constant, T is the experimental temperature, and A is the Arrhenius prefactor. **Fig. 3B** shows the Arrhenius analysis of τ^* versus 1000/T. The calculated E_a of the DGEAC/AFD networks (R = 0.5) is 109 kJ mol^{-1} according to the slope of the Arrhenius plot. Meanwhile, the topology freezing transition temperature (T_v) was determined to be 114 °C using the Maxwell's

equation (**Fig. S4**). Note that the bond exchange reactions in the DGEAC/AFD networks were also affected by the segment mobility (related to T_g), considering that T_v was lower than T_g. That is to say, the exchange reactions can occur and cause stress relaxation even if the motion of polymer chains was slow. When the temperature was above T_g, its stress relaxation became fast (τ^* = 28 s, 230 °C). Furthermore, the creep recovery behavior of the DGEAC/AFD networks is shown in **Fig. 3C**. After an initial elastic response at 200 °C, the networks flowed, driven by the disulfide bonds exchange and TERs, and the strain increased to 9.3% until the stress was revoked after 60 min, followed by a slight decrease and retention of elongation of 8.0% in the remaining time.

Owing to its intrinsic dynamic nature, the cross-linked network of DGEAC/AFD can react with molecules such as DTT to produce broken chain segments, degrading the networks. Herein, the degradation kinetics of the DGEAC/AFD networks (R = 0.5) were investigated in a DMF solution of DTT at 70 °C by monitoring the residual weight of the sample. As shown in **Fig. 3D**, after a swelling period for the first 6 h, the block begins to degrade, and disappears completely after 20 h. The degradation rate is dominated by the following processes: 1) DTT molecules diffuse into the polymer networks, 2) polymer chains was broken into segments due to the thiol-disulfide reaction and the transesterification reactions, and 3) the broken segments diffuse into the DMF solvent (**Fig. 3F**). Because of the high cross-linking density and rigid networks, the diffusion rate of DTT into the DGEAC/AFD networks was low, and the total degradation time reached up to 20 h.

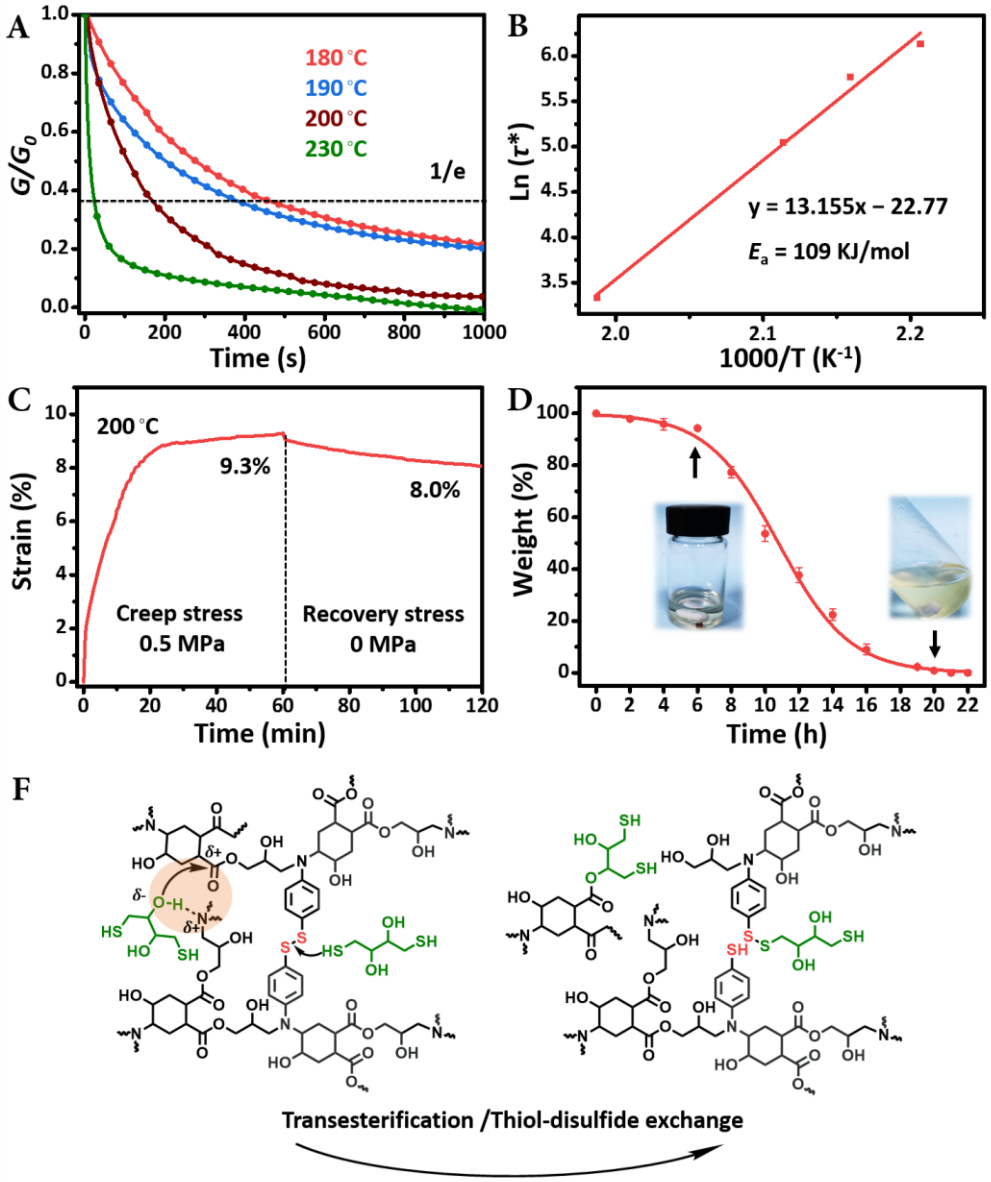

Fig. 3. (A) Stress relaxation curves of DGEAC/AFD networks (R = 0.5) at different temperatures. (B) Linear fitting curve of the relaxation times (τ*) derived from (A) to an Arrhenius-type equation. (C) Creep recovery behavior of DGEAC/AFD networks (R = 0.5) at 200 °C. (D) Degradation kinetics of DGEAC/AFD networks (R = 0.5) in DTT/DMF solution at 70 °C. Inset image showed the sample before and after degradation. (E) Proposed degradation mechanism of DGEAC/AFD networks in the presence of DTT molecules.

3.4 Mechanochromic properties of DGEAC/AFD networks

Fig. 4A shows the mechanochromic behavior of the DGEAC/AFD networks. When the DGEAC/AFD networks was carved with a knife, the location color immediately changed to green, which could be clearly observed by the naked eye. After placing the carved powder at room temperature for 24 h, the color changed back to the original (**Fig. 4B**). It is worth noting that there was no apparent color change on the fracture surface of the resin after tensile and flexural fracture (**Fig. S5**). To investigate this behavior in detail, the EPR spectrum of the green DGEAC/AFD powder was first studied (**Fig. 4C**). The three anisotropic EPR signals at $g_1 = 2.0032$, $g_2 = 2.0197$, and $g_3 = 2.0407$ belong to the sulfenyl radicals generated from the cleavage of disulfide bonds [67]. The Raman spectra are shown in **Fig. 4D**. Compared with the intact DGEAC/AFD networks exhibiting peaks at 472 and 640 cm^{-1} for the S-S and C-S bonds, respectively, a new peak appears at 600 cm^{-1} for the green DGEAC/AFD powder, which should be assigned to sulfenyl radicals [68]. Such radicals, being 'frozen' in the polymer networks with a high T_g, survive for some time before pairing up to form disulfide bonds, which could explain the progressive disappearance of the green color after several hours.

To further evaluate the stability of such radicals, the duration of retention of the green color at different temperatures was quantified by UV-vis spectroscopy in the solid state. As shown in **Fig. 4E**, a peak at 652 nm corresponding to the green color is observed, the intensity of which progressively decreases to zero within 20 h at 25 °C due to the recombination of sulfenyl radicals to form disulfide bonds. In contrast, upon storing the green powder at 70 °C and 100 °C, the absorption peak at 652 nm decreases more rapidly (**Fig. S6**). Here, the time is defined as the duration of color retention ($t_{1/2}$) when the absorbance intensity (A_t) is 1/2 of the initial intensity (A_0) at 652 nm. As shown in **Fig. 4F**, the $t_{1/2}$ values are 180, 28, and 5 min for the green

DGEAC/AFD powder at 25 °C, 70 °C, and 100 °C, respectively. This can be explained by the high mobility of polymer segments at high temperatures, resulting in the fast pairing of radical species. Notably, despite being reactive, these sulfenyl radicals can be 'frozen' and survive for a while when the temperature is far below T_g, providing sufficient time for self-reporting and analyzing damage in the matrix and composites.

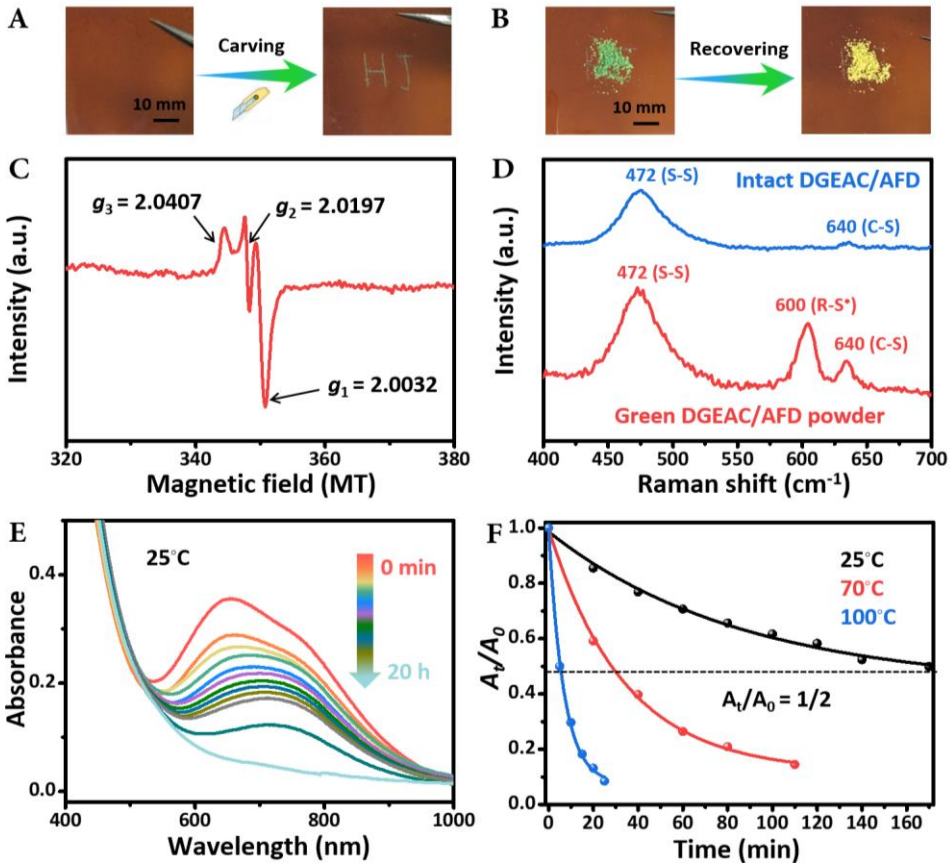

Fig. 4. (A) Mechanochromic behavior of DGEAC/AFD networks (R = 0.5) upon carving and (B) recovery from green to the original color after standing at room temperature for 24 h. (C) EPR spectrum of the green DGEAC/AFD powder (R = 0.5). (D) Raman spectrum of the DGEAC/AFD networks (R = 0.5) and the carved green DGEAC/AFD powder (R = 0.5). (E) Time-dependent UV-vis spectra of the green DGEAC/AFD powder (R = 0.5) at 25 °C. (F) Normalized time-

dependent UV-vis spectra of the green DGEAC/AFD powder (R = 0.5) at different temperatures. A_0 is the initial absorbance intensity at 652 nm and A_t is the absorbance intensity at the test time.

3.5 Preparation and periodic impact test of GF/DGEAC/AFD composites

DGEAC/AFD networks (R = 0.5) were selected as the matrix and GFs (EW250F) as the reinforcing fibers, and the GF/DGEAC/AFD composites were prepared by dip-coating (**Scheme 1B**). The cured composite laminates are shown in **Fig. 5A**, where the mass fraction of GFs is approximately 71%. An X-ray 3D microscope was used to study internal structures of dimensions 10 mm × 10 mm × 1 mm. The satin structures of the woven GFs could be captured in the integral and cross-sectional images (**Fig. 5B**, **5D)**. The cross-sectional XY and XZ micrographs (**Fig. 5C**, **5E**) showed no signs of delamination or porosity between the GFs and polymer matrix, revealing the good interfacial properties of the composites. Moreover, the SEM results showed that after merging with the DGEAC/AFD matrix, a robust interface between the matrix and GFs was formed, where the GFs were tightly enclosed by the matrix (**Fig. 5F**). In addition, tensile and flexural tests were performed to investigate the mechanical properties of the GF/DGEAC/AFD composites. The tensile strength and Young's modulus were 470.5 MPa and 13.0 GPa (**Fig. 5G, 5I**), while the flexural strength and corresponding modulus were 726.4 MPa and 12.2 GPa (**Fig. 5H**, **5I**). To intuitively illustrate the high performance of the GF/DGEAC/AFD composites, a comparison of the tensile strengths of GF/DGEAC/AFD and other reported epoxy-based GFRCs is provided in **Table S4**; the GF/DGEAC/AFD composites show a higher mechanical strength.

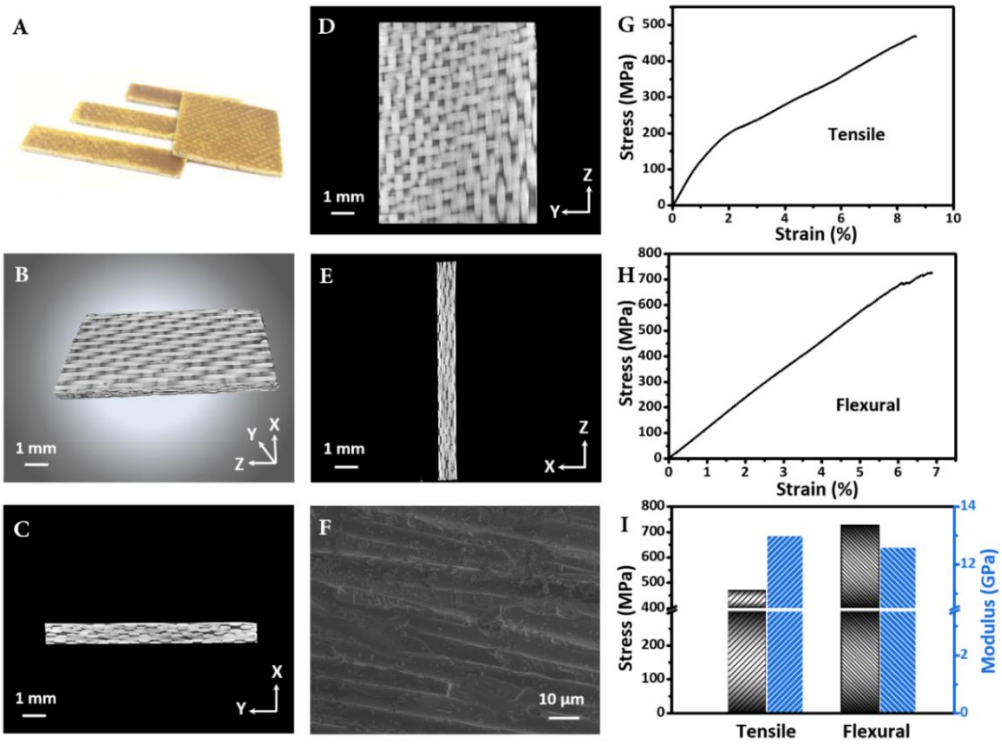

Fig. 5. (A) Optical photograph of GF/DGEAC/AFD composites. X-ray 3D microscopic (B) integral, (C) XY, (D) YZ, and (E) XZ cross-profile images of the GF/DGEAC/AFD composites. (F) SEM image of the plane surface of GF/DGEAC/AFD composites. (G) Tensile and (H) flexural stress-strain curves of GF/DGEAC/AFD composites, and (I) corresponding stress and modulus values.

Benefiting from the mechanochromic features of the DGEAC/AFD matrix, the intrinsic damage self-reporting property of the GF/DGEAC/AFD composites was evaluated using a custom 'hammer impact' test (**Fig. S7**), which yielded an impact energy of ~0.598 J for each hit. To track the color change and failure of the GF/DGEAC/AFD composites, images were captured after each impact. As shown in **Fig. 6A**, with increasing impact number, the green color on the impact location gradually intensifies. A color change visible to the naked eye is seen at the 4th impact (image 4), while the cracks in the composites do not appear until the 70th impact (image 70), where

the fiber fractures on the surface and inside of the composite are observed in SEM (**Fig. 6B**) and X-ray 3D images (**Fig. S8**). In other words, a color change appears before the composites fail, revealing the intrinsic damage self-reporting capability of the GF/DGEAC/AFD composites. To precisely quantify the color change, the average brightness of the blue channel at the impact location was tracked using ImageJ software. The accumulated impact energy corresponding to the impact numbers is plotted against the blue color contribution (**Fig. 6C**, **Movie S1**), with a standard blue scale bar as a reference. For the first two impacts, the color development is slight, whereas from the 2nd to 4th impacts, a distinct color change is observed (2.39 J). With the progress of the periodic impact test, the color change progresses steadily until the material fails at the 70th impact point (41.86 J). Obviously, the GF/DGEAC/AFD composites exhibit notable color development before severe material damage. Similar to neat resin, no color change of the GF/DGEAC/AFD composites was observed after tensile fracture, while only a slight color change at the stress point in flexural test (**Fig. S9**), which might be probably because the fracture of disulfide bonds requires a specific type of stress, such as knife carving, impact, etc., to generate enough free radicals for visualization.

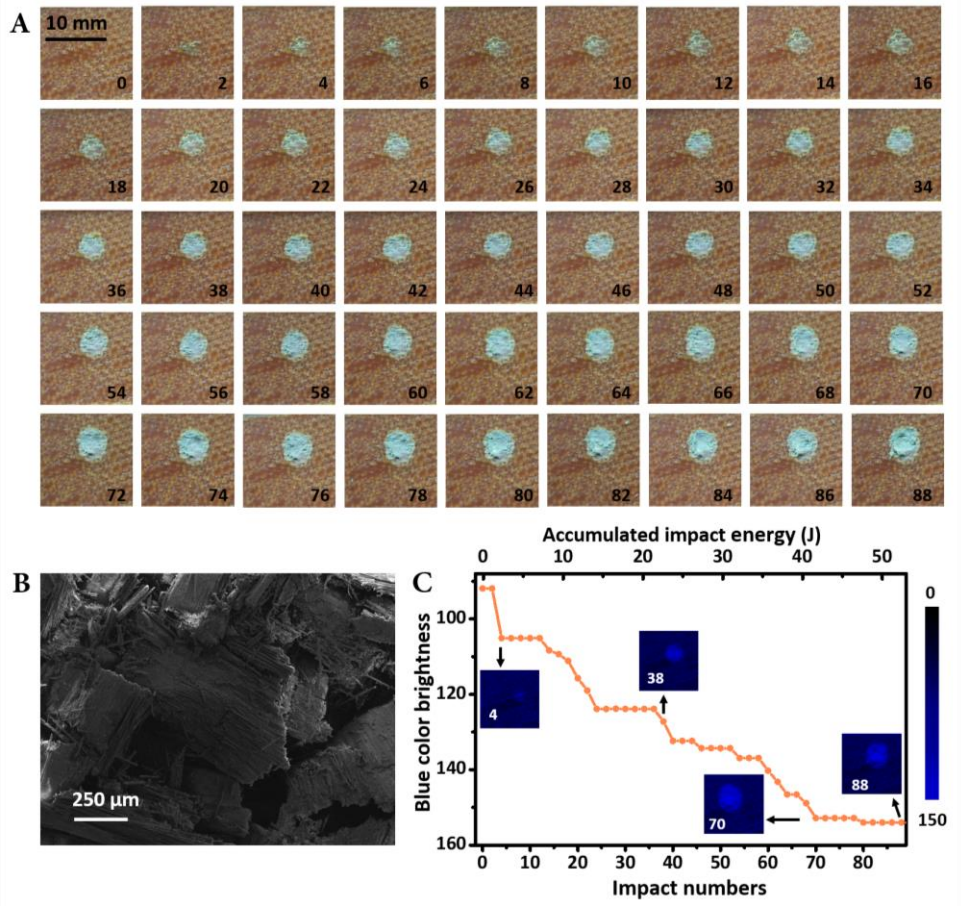

Fig. 6. (A) Periodic 'hammer impact' of GF/DGEAC/AFD composites. The number in each image represents the impact numbers. Images were captured immediately after each impact. (B) SEM image of the impact surface of the GF/DGEAC/AFD composites at the 70th impact. (C) Quantitative analysis of the color changes and accumulated energy after periodic impacts.

3.6 Recycling of GF/DGEAC/AFD composites

Based on the bond exchange reaction between thiol and disulfide, as well as the transesterification reactions catalyzed by internal tertiary amines, DTT was chosen as the degradation agent for the GF/DGEAC/AFD composites in the DMF solution at 70 °C. The digital photos in **Fig. 7A** provide indirect evidence of the recycling process. The solution color deepens as the incubation time increases with the separation of GF layers, and the matrix of DGEAC/AFD

is completely removed after 40 h, affording recycled GFs. The degradation kinetics were investigated by measuring the residual weight at different degradation times. As shown in **Fig. 7B**, the weight decreases to 88% in the first 9 h, reaches 78% at 20 h, and finally decreases to 70% at 40 h, approaching the actual weight of the GF/DGEAC/AFD composites (71%). SEM images were acquired to further monitor the degradation process (**Fig. 7C**). At 0 h, there is a robust interface between the DGEAC/AFD matrix and GFs; after 9 h, only a small part of the matrix is degraded; after 24 h, a large amount of the matrix depolymerises, causing more GFs to be exposed. Consequently, all matrices are removed from the GFs after 40 h. Note that because of the good interface combination between the GFs and matrix, a long soaking time was required to allow sufficient DTT molecules to enter the composite interior. The SEM images in **Fig. S10** reveal that the recycled GFs exhibit a clean and smooth surface, identical to that of the virgin GFs. In addition, the SEM-EDS results indicate that the recycled GFs have a similar composition as that of the virgin GFs (**Fig. S11**, **Table S5**). This implies that the degradation process hardly affects the properties of recycled GFs. Given above, degradation process is shown in **Fig. 7D**. Initially, the DGEAC/AFD matrix swells with the introduction of DTT into the cross-linked network (i). Subsequently, the thiol groups and hydroxyl groups of DTT participate in the exchange reactions at 70 °C, leading to the partial degradation of the DGEAC/AFD networks (ii). Finally, all disulfide bonds and ester bonds in the networks are degraded by DTT, affording clean recycled GFs (iii).

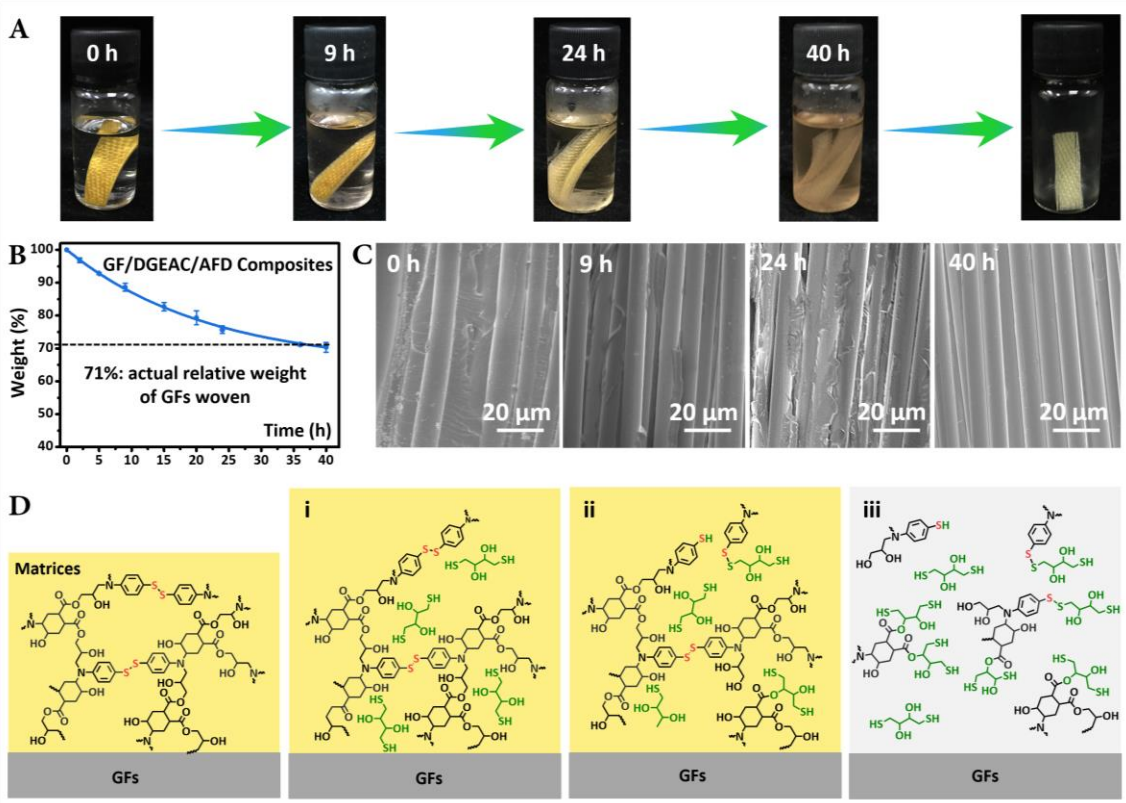

Fig. 7. (A) Digital photos and (B) degradation kinetics of GF/DGEAC/AFD composites in a DTT/DMF solution at 70 °C. (C) SEM images of the cleavage plane of GF/DGEAC/AFD composites degradation times of 0, 9, 24, and 40 h. (D) Proposed degradation process of GF/DGEAC/AFD composites: (i) the matrix swells in a DTT/DMF solution at 70 °C; (ii) the matrix partially degrades due to the thiol groups and hydroxyl groups of DTT participate in the exchange reactions at 70 °C; (iii) the matrix completely degrades and is removed from the GFs.

4. Conclusions

Disulfide bond-tailored epoxy networks with different stoichiometric ratios of amine/epoxy groups were prepared from DGEAC and AFD. These networks exhibited sufficient solvent resistance, good thermal and mechanical properties ($T_g \geq 206°$ C, $T_{d5\%} \geq 270$ °C, tensile strength ≈ 70 MPa, and Young′s modulus ≈ 1.61 GPa), and UV-shielding ability. Because of the exchange

reaction of disulfide bonds and dynamic transesterification reactions catalyzed by internal tertiary amines, the DGEAC/AFD networks could rearrange at 200 °C with a short stress relaxation time of 156 s and E_a of 109 kJ mol^{-1}, undergo creep at 200 °C, and easily degrade in a DTT solution. More importantly, the DGEAC/AFD networks showed intrinsic mechanochromic properties because of the generation of sulfenyl radicals in the damage location, where the color immediately changed to green, as observed by the naked eye. Owing to the good comprehensive performance of the DGEAC/AFD matrix, the GF/DGEAC/AFD composites exhibited outstanding mechanical properties (tensile strength of ~470 MPa, Young′s modulus of 13.0 GPa, flexural strength of ~726 MPa, and corresponding modulus of 12.2 GPa). Remarkably, the GF/DGEAC/AFD composites could self-report damage over time with the appearance of a green color owing to the intrinsic mechanochromic properties of the epoxy matrix. Thus, the degree of damage caused by impact could be accurately evaluated to indicate material failure. Finally, the GFs could be completely recycled in a non-destructive manner by immersing the GF/DGEAC/AFD composites in a DTT solution. This research provides an alternative strategy to fabricate high-performance, damage-indicative, UV-shielding, and fully recyclable GFRCs.

Declaration of competing interest

The authors declare that they have no known competing financial interests or personal relationships that could have appeared to influence the work reported in this paper.

Acknowledgements

This work is supported by the Open Fund of National Key Laboratory of Science and Technology on Advanced Composite (KZ42191814). The authors wish to thank Mr. Fuzheng Ji from the Composite Testing Technology Center of AVIC Composite Co., Ltd for his help with the X-ray 3D microscopy testing.

Appendix A. Supplementary data

Supplementary data to this article can be found online.

References

[1] Y. Liu, G. Liu, Y. Li, Y. Weng, J. Zeng, Biobased high-performance epoxy vitrimer with UV shielding for recyclable carbon fiber reinforced composites, ACS Sustain. Chem. Eng. 9(12) (2021) 4638-4647, https://pubs.acs.org/doi/10.1021/acssuschemeng.1c00231.

[2] O.R. -Graham, E.A. Apebende, L.K. Bast, N. Bruns, Self-reporting fiber-reinforced composites that mimic the ability of biological materials to sense and report damage, Adv. Mater. 30(19) (2018) 1705483, https://doi.org/10.1002/adma.201705483.

[3] G. Marsh, Meeting the challenge of wind turbine blade repair, Reinf. Plast. 55(4) (2011) 32-36, https://doi.org/10.1016/S0034-3617(11)70112-6.

[4] H.Y. Hwang, Effect of the crack length on the piezoelectric damage monitoring of glass fiber epoxy composite DCB specimens, Compos. Sci. Technol. 72(8) (2012) 902-907, https://doi.org/10.1016/j.compscitech.2012.02.022.

[5] L. Friedrich, A. Colpo, A. Mgggi, T. Becker, G. Lacidogna, I. Iturrioz, Damage process in glass fiber reinforced polymer specimens using acoustic emission technique with low frequency acquisition, Compos. Struct. 256 (2021) 113105, https://doi.org/10.1016/j.compstruct.2020.113105.

[6] W. Zhou, W. Zhao, Y. Zhang, Z. Ding, Cluster analysis of acoustic emission signals and deformation measurement for delaminated glass fiber epoxy composites, Compos. Struct. 195 (2018) 349-358, https://doi.org/10.1016/j.compstruct.2018.04.081.

[7] A. Nair, C.S. Cai, X. Kong, Acoustic emission pattern recognition in CFRP retrofitted RC beams for failure mode identification, Compos. Pt. B-Eng. 161(15) (2019) 691-701, https://doi.org/10.1016/j.compositesb.2018.12.120.

[8] D. Stifter, K. Wiesauer, M. Wurm, E. Schlotthauer, J. Kastner, M. Pircher, E. Götzinger, C.K. Hitzenberger, Investigation of polymer and polymer/fibre composite materials with optical coherence tomography, Meas. Sci. Technol. 19(7) (2008) 074011, https://iopscience.iop.org/article/10.1088/0957-0233/19/7/074011.

[9] K. Wiesauer, M. pircher, E. Goetzinger, C.K. Hitzenberger, R. Oster, D. Stifter, Investigation of glass-fibre reinforced polymers by polarisation-sensitive, ultra-high resolution optical coherence tomography: Internal structures, defects and stress, Compos. Sci. Technol. 67(15-16) (2007) 3051-3058, https://doi.org/10.1016/j.compscitech.2007.04.018.

[10] B.C.F. Oliveira, A.A. Seibert, D. Staub, A. Albertazzi, Square-pulse shearography inspections of metallic parts repaired with a glass fiber reinforced polymer using pressure, radiation, vibration, and induction loading methods, Int. J. Pres. Ves. Pip. 187 (2020) 104187, https://doi.org/10.1016/j.ijpvp.2020.104187.

[11] Y.Y. Hung, W.D. Luo, L. Lin, H.M. Shang, Evaluating the soundness of bonding using shearography, Compos. Struct. 50(4) (2000) 353-362, https://doi.org/10.1016/S0263-8223(00)00109-4.

[12] N. Tao, A.G. Anisimov, R.M. Groves , Shearography non-destructive testing of thick GFRP laminates: Numerical and experimental study on defect detection with thermal loading, Compos. Struct. 282 (2021), 115008, https://doi.org/10.1016/j.compstruct.2021.115008.

[13] C. Xu, W. Zhang, C. Wu, J Xie, X. Ying, G. Chen, An improved method of eddy current pulsed thermography to detect subsurface defects in glass fiber reinforced polymer composites, Compos. Struct. 242 (2020) 112145, https://doi.org/10.1016/j.compstruct.2020.112145.

[14] R.D. Crouch, S.B. Clay, C. Oskay, Experimental and computational investigation of progressive damage accumulation in CFRP composites, Compos. Pt. B-Eng. 48 (2013) 59-67, https://doi.org/10.1016/j.compositesb.2012.12.005.

[15] C.J. Hansen, W. Wu, K.S. Toohey, N.R. Sottos, S.R. White, J.A. Lewis, Self-healing materials with interpenetrating microvascular networks, Adv. Mater. 21(41) (2009) 4143-4147, https://doi.org/10.1002/adma.200900588.

[16] K.S. Toohey, N.R. Sottos, J.A. Lewis, J.S. Moore, S.R. White, Self-healing materials with microvascular networks, Nat. Mater. 6(8) (2007) 581-585, https://doi.org/10.1038/nmat1934.

[17] J.F. Patrick, K.R. Hart, B.P. Krull, C. E. Diesendruck, J.S. Moore, S.R. White, N.R. Sottos, Self-healing: continuous self-healing life cycle in vascularized structural composites, Adv. Mater. 26(25) (2014) 4302-4308, https://doi.org/10.1002/adma.201470166.

[18] S.R. White, N.R. Sottos, P.H. Geubelle, J.S. Moore, M.R. Kessler, S.R. Sriram, E.N. Brown, S. Viswanathan, Autonomic healing of polymer composites, Nature 409(6822) (2001) 794-791, https://doi.org/10.1038/35057232.

[19] S. Vidinejevs, O. Strekalova, A. Aniskevich, S. Gaidukov, Development of a composite with an inherent function of visualization of a mechanical action, Mech. Compos. Mater. 49(1) (2013) 77-84, https://doi.org/10.1007/s11029-013-9323-9.

[20] W. Li, C.C Matthews, K Yang, M.T Odarczenko, S.R White, N.R Sottos, Autonomous indication of mechanical damage in polymeric coatings, Adv. Mater. 28(11) (2016) 2189-2194, https://doi.org/10.1002/adma.201505214.

[21] S.M. Bleay, C.B. Loader, V.J. Hawyes, L. Humberstone, P.T Curtis, A smart repair system for polymer matrix composites, Compos. Pt. A-Appl. Sci. Manuf. 32(12) (2001) 1767-1776, https://doi.org/10.1016/s1359-835x(01)00020-3.

[22] J.W.C. Pang, I.P. Bond, 'Bleeding composites′—damage detection and self-repair using a biomimetic approach, Compos. Pt. A-Appl. Sci. Manuf. 36(2) (2005) 183-188, https://doi.org/10.1016/j.compositesa.2004.06.016.

[23] S. Klinga, T. Czigany, Damage detection and self-repair in hollow glass fiber fabric-reinforced epoxy composites via fiber filling, Compos. Sci. Technol. 99(4) (2014) 82-88, https://doi.org/10.1016/j.compscitech.2014.05.020.

[24] V.M. Diep, A.M. Armani, Flexible light-emitting nanocomposite based on ZnO nanotetrapods, Nano Lett. 16(12) (2016) 7389-7393, https://doi.org/10.1021/acs.nanolett.6b02887.

[25] X. Jin, M Gotz, S. Wille, Y.K. Mishra, R. Adelung, C. Zollfrank, A novel concept for self-reporting materials: stress sensitive photoluminescence in ZnO tetrapod filled elastomers, Adv. Mater. 25(9) (2013) 1342-1347, https://doi.org/10.1002/adma.201203849.

[26] S. Shree, M. Dowds, A. Kuntze, Y.K. Mishra, A. Staubitz, R. Adelung, Self-reporting mechanochromic coating: a glassfiber reinforced polymer composite that predicts impact induced damage, Mater. Horiz. 7(2) (2020) 598-604, https://doi.org/10.1039/C9MH01400D.

[27] T. Chen, C.D. Mansfield, L. Ju, D.G. Baird, The influence of mechanical recycling on the properties of thermotropic liquid crystalline polymer and long glass fiber reinforced polypropylene, Compos. Part. B-Eng. 200 (2020) 108316, https://doi.org/10.1016/j.compositesb.2020.108316.

[28] P.-A. Eriksson, A.-C. Albertsson, P. Boydell, G. Prautzsch, J.-A.E. Manson, Prediction of mechanical properties of recycled fiberglass reinforced polyamide 66, Polym. Compos. 17(6) (1996) 830-839, https://doi.org/10.1002/pc.10676.

[29] G. Oliveux, L.O. Dandy, G.A. Leeke, Current status of recycling of fibre reinforced polymers: Review of technologies, reuse and resulting properties, Prog. Mater. Sci. 72 (2015) 61-99, https://doi.org/10.1016/j.pmatsci.2015.01.004.

[30] R.S. Ginder, S. Ozcan, Recycling of commercial e-glass reinforced thermoset composites via two temperature step pyrolysis to improve recovered fiber tensile strength and failure strain, Recycling 4(2) (2019) 24, https://doi.org/10.3390/recycling4020024.

[31] M. Rani, P. Choudhary, V. Krishnan, S. Zafar, A review on recycling and reuse methods for carbon fibre/glass fibre composites waste from wind turbine blades, Compos. Part. B-Eng. 215 (2021) 108768, https://doi.org/10.1016/j.compositesb.2021.108768.

[32] Y. Qiao, O. Das, S. Zhao, T. Sun, Q. Xu, L. Jiang, Pyrolysis kinetic study and reaction mechanism of epoxy glass fiber reinforced plastic by thermogravimetric analyzer (TG) and TG–FTIR (Fourier-Transform Infrared) techniques, Polymers 12(11) (2020) 2739, https://doi.org/10.3390/polym12112739.

[33] C.J. Kloxin, T.F. Scott, B.J. Adzima, C.N. Bowman, Covalent adaptable networks (CANs): a unique paradigm in cross-linked polymers, Macromolecules 43(6) (2010) 2643-2653, https://doi.org/10.1021/ma902596s.

[34] D. Montarnal, M. Capelot, F. Tournilhac, L. Leibler, Silica-Like Malleable Materials From Permanent Organic Networks, Science 334(965) (2011) 965-968, https://doi.org/10.1126/science.1212648.

[35] B. Ren, D. Zhao, S. Liu, X. Liu, Z. Tong, Synthesis and characterization of poly(ferrocenylsilanes) with coumarin side groups and their photochemical reactivity and electrochemical behavior, Macromolecules 40(13) (2007) 4501-4508, https://doi.org/10.1021/ma062502o.

[36] A. Khan, N. Ahmed, M. Rabnawaz, Covalent Adaptable Network and Self-Healing Materials: Current Trends and Future Prospects in Sustainability, Polymers 12(9) 2020 2027, https://doi.org/10.3390/polym12092027.

[37] K. Yu , Q. Shi , M. L. Dunn, T. Wang, H. J. Qi, Carbon fiber reinforced thermoset composite with near 100% recyclability, Adv. Funct. Mater. 26 (33) (2016) 6098–6106, https://doi.org/10.1002/adfm.201602056.

[38] Q. Li, S. Ma, P. Li, B. Wang, Z. Yu, H. Feng, Y. Liu, J. Zhu, Fast reprocessing of acetal covalent adaptable networks with high performance enabled by neighboring group participation, Macromolecules 54(18) (2021) 8423-8434, https://doi.org/10.1021/acs.macromol.1c01046.

[39] S. Wang, S. Ma, Q. Li, X. Xu, B. Wang, W. Yuan, S. Zhou, S. You, J Zhu, Facile in situ preparation of high-performance epoxy vitrimer from renewable resources and its application in nondestructive recyclable carbon fiber composite, Green Chem. 21(6) (2019) 1484-1497, https://doi.org/10.1039/C8GC03477J.

[40] H. Si, L. Zhou, Y. Wu, L. Song, M. Kang, X. Zhao, M. Chen, Rapidly reprocessable, degradable epoxy vitrimer and recyclable carbon fiber reinforced thermoset composites relied on high contents of exchangeable aromatic disulfide crosslinks, Compos. Part. B-Eng 199 (2020) 108278, https://doi.org/10.1016/j.compositesb.2020.108278.

[41] M. Chen, L. Zhou, Y. Wu, X. Zhao, Y. Zhang, Rapid stress relaxation and moderate temperature of malleability enabled by the synergy of disulfide metathesis and carboxylate transesterification in epoxy vitrimers. ACS Macro Lett. 8(3) (2019) 255-260, https://doi.org/10.1021/acsmacrolett.9b00015.

[42] I. Azcune, I. Odriozola, Aromatic disulfide crosslinks in polymer systems: Self-healing, reprocessability, recyclability and more, Eur. Polym. J. 84 (2016) 147-160, https://doi.org/10.1016/j.eurpolymj.2016.09.023.

[43] H. Memon, H. Liu, M.A. Rashid, L. Chen, Q. Jiang, L. Zhang, Y. Wei, W. Liu,Y. Qiu, Vanillin-based epoxy vitrimer with high performance and closed-loop recyclability, Macromolecules 53(2) (2020) 621-630, https://doi.org/10.1021/acs.macromol.9b02006.

[44] Y. Liu, B. Wang, S. Ma, T. Yu, X. Xu, Q. Li, S. Wang, Y. Han, Z. Yu, J. Zhu, Catalyst-free malleable, degradable, bio-based epoxy thermosets and its application in recyclable carbon fiber composites, Compos. Pt. B-Eng. 211(3) (2021) 108654, https://doi.org/10.1016/j.compositesb.2021.108654.

[45] S. Ma, D.C. Webster, F. Jabeen, Hard and flexible, degradable thermosets from renewable bioresources with the assistance of water and ethanol, Macromolecules 49(10) (2016) 3780-3788, https://doi.org/10.1021/acs.macromol.6b00594.

[46] S. Ma, D.C. Webster, Naturally occurring acids as cross-linkers to yield voc-free, high-performance, fully bio-based, degradable thermosets, Macromolecules 48(19) (2015) 7127-7137, https://doi.org/10.1021/acs.macromol.5b01923.

[47] X. Xu, S. Ma, S. Wang, J. Wu, Q. Li, N. Lu, Y. Liu, J. Yang, J.Feng, J. Zhu, Dihydrazone-based dynamic covalent epoxy networks with high creep resistance, controlled degradability, and intrinsic antibacterial properties from bioresources, J. Mater. Chem. A 8(22) (2020) 11261-11274, https://doi.org/10.1039/D0TA01419B.

[48] Q. Li, S. Ma, P. Li, B. Wang, Z. Yu, H. Feng, Y. Liu, J. Zhu, Fast reprocessing of acetal covalent adaptable networks with high performance enabled by neighbouring group participation, Macromolecules 54(18) (2021) 8423-8434, https://doi.org/10.1021/acs.macromol.1c01046.

[49] Y. Liu, J. He, Y. Li, X. Zhao, J. Zeng, Biobased, reprocessable and weldable epoxy vitrimers from epoxidized soybean oil, Ind. Crops Prod. 153 (2020) 112576, https://doi.org/10.1016/j.indcrop.2020.112576.

[50] X. Yang, S. Wang, X. Liu, Z. Huang, X. Huang, X. Xu, H. Liu, D. Wang, S. Shang, Preparation of non-isocyanate polyurethanes from epoxy soybean oil: dual dynamic networks to realize self-healing and reprocessing under mild conditions, Green Chem. 23(17) (2021) 6349-6355, https://doi.org/10.1039/D1GC01936H.

[51] X. Feng, G. Li, Room-temperature self-healable and mechanically robust thermoset polymers for healing delamination and recycling carbon fibers, ACS Appl. Mater. Interfaces, 13(44) (2021) 53099-53110, https://doi.org/10.1021/acsami.1c16105.

[52] S. Wang, S. Ma, Q. Li, W. Yuan, B. Wang, J. Zhu, Robust, fire-safe, monomer-recovery, highly malleable thermosets from renewable bioresources, Macromolecules 51(20) (2018) 8001-8012, https://doi.org/10.1021/acs.macromol.8b01601.

[53] S. Zhao, M.M. Abu-Omar, Recyclable and malleable epoxy thermoset bearing aromatic imine bonds, Macromolecules 51 (23) (2018) 9816–9824, https://doi.org/10.1021/acs.macromol.8b01976.

[54] Y. Xu, S. Dai, H. Zhang, L. Bi, J. Jiang, Y. Chen, Reprocessable, self-adhesive, and recyclable carbon fiber-reinforced composites using a catalyst-free self-healing bio-based vitrimer matrix, ACS Sustain. Chem. Eng. 9(48) (2021) 16281-16290, https://doi.org/10.1021/acssuschemeng.1c05586.

[55] K. Hong, Q. Sun, X. Zhang, L. Fan, T. Wu, J. Du, Y. Zhu, Fully bio-based high-performance thermosets with closed-loop recyclability, ACS Sustain. Chem. Eng. 10(2) 2022 1036-1046, https://doi.org/10.1021/acssuschemeng.1c07523.

[56] H. Memon, Y. Wei, L. Zhang, Q. Jiang, W. Liu, An imine-containing epoxy vitrimer with versatile recyclability and its application in fully recyclable carbon fiber reinforced composites, Compos. Sci. Technol. 199 (2020) 108314, https://doi.org/10.1016/j.compscitech.2020.108314.

[57] Y. Xu, S. Dai, L. Bi, J. Jiang, H. Zhang, Y. Chen, Catalyst-free self-healing bio-based vitrimer for a recyclable, reprocessable, and self-adhered carbon fiber reinforced composite, Chem. Eng. J. 429 (2022) 132518, https://doi.org/10.1016/j.cej.2021.132518.

[58] A. R. de Luzuriaga, R. Martin, N. Markaide, A. Rekondo, G. Cabanero, J. Rodríguez and I. Odriozola, Epoxy resin with exchangeable disulfide crosslinks to obtain reprocessable, repairable and recyclable fiber-reinforced thermoset composites, Mater. Horiz., 3(3) (2020) 241–247, https://doi.org/10.1039/C6MH00029K.

[59] C. Hao, T. Liu, S. Zhang, W. Liu, Y. Shan, J. Zhang, Triethanolamine-mediated covalent adaptable epoxy network: excellent mechanical properties, fast repairing, and easy recycling, Macromolecules 53(8) (2020) 3110-3118, https://doi.org/10.1021/acs.macromol.9b02243.

[60] S. Ma, J. Wei, Z. Jia, T. Yu, W. Yuan, Q. Li, S. Wang, S. You, R. Liu, J. Zhu, Readily recyclable, high-performance thermosetting materials based on a ligninderived spiro diacetal trigger, J. Mater. Chem. A 7(3) (2019) 1233–1243, https://doi.org/10.1039/C8TA07140C.

[61] X. Xu, S. Ma, J. Wu, J. Yang, B. Wang, S. Wang, Q. Li, J. Feng, S. You, J Zhu, High-performance, command-degradable, antibacterial Schiff base epoxy thermosets: synthesis and properties, J. Mater. Chem. A 7(25) (2019) 15420-15431, https://doi.org/10.1039/C9TA05293C.

[62] S. You, S. Ma, J. Dai, Z. Jia, X. Liu, J Zhu, Hexahydro-s-triazine: A trial for acid-degradable epoxy resins with high performance, ACS Sustain. Chem. Eng. 5(6) 4683-4689, https://doi.org/10.1021/acssuschemeng.7b00030.

[63] Y. Tao, L. Fang, Me. Dai, C. Wang, J. Sun, Q. Fang, Sustainable alternative to bisphenol A epoxy resin: high-performance recyclable epoxy vitrimers derived from protocatechuic acid, Polym. Chem. 11(27) (2020) 4500-4506, https://doi.org/10.1039/D0PY00545B.

[64] C. Taplan, M. Guerre, F. E. Du Prez, Covalent adaptable networks using β-amino esters as thermally reversible building blocks, J. Am. Chem. Soc. 143(24) (2021) 9140-9150, https://doi.org/10.1021/jacs.1c03316.

[65] F. Van Lijsebetten, J.O. Holloway, J.M. Winne, F.E. Du Prez, Internal catalysis for dynamic covalent chemistry applications and polymer science, Chem. Soc. Rev. 49(23) (2020) 8425-8438, https://doi.org/10.1039/D0CS00452A.

[66] F. Cuminet, S. Caillol, É. Dantras, É. Leclerc, V. Ladmiral, Neighboring group participation and internal catalysis effects on exchangeable covalent bonds: application to the thriving field of vitrimer chemistry, Macromolecules 54(9) 2021 3927-3961, https://doi.org/10.1021/acs.macromol.0c02706.

[67]Y. Amamoto, H. Otsuka, A. Takahara, K. Matyjaszewski, Self-healing of covalently cross-linked polymers by reshuffling thiuram disulfide moieties in air under visible light, Adv. Mater. 24(29) (2012) 3975-3980, https://doi.org/10.1002/adma.201201928.

[68] G. Zhang, H. Peng, C. Zhao, X. Chen, L. Zhao, P. Li, J. Huang, Q. Zhang, The radical pathway based on a lithium-metal-compatible high-dielectric electrolyte for lithium-sulfur batteries, Angew. Chem. Int. Edit. 57(51) (2018) 16732-16736, https://doi.org/10.1002/anie.201810132.